

Identification of hypoxic-related lncRNAs prognostic model for revealing clinical prognostic and immune infiltration characteristic of cutaneous melanoma

Congjuan Liao¹, Jiabao Yang¹, Liuting Chen², Zhiguang Ye¹

¹Dermatology and STD Department of The Second Affiliated Hospital, School of Medicine, The Chinese University of Hong Kong, Shenzhen and Longgang District People's Hospital of Shenzhen, Shenzhen 518172, China

²Beijing University of Chinese Medicine Shenzhen Hospital (Long Gang), Shenzhen 518116, China

Correspondence to: Zhiguang Ye; **email:** 201010130510@stu.swmu.edu.cn

Keywords: cutaneous melanoma, hypoxia, immune infiltration, risk stratification, immunotherapy evaluation

Received: September 8, 2023

Accepted: December 26, 2023

Published: February 15, 2024

Copyright: © 2024 Liao et al. This is an open access article distributed under the terms of the [Creative Commons Attribution License](https://creativecommons.org/licenses/by/4.0/) (CC BY 4.0), which permits unrestricted use, distribution, and reproduction in any medium, provided the original author and source are credited.

ABSTRACT

Background: Cutaneous melanoma (CM) remains a significant threat to human health. There are clues to the potential role of hypoxia in CM progression. However, the role of hypoxia-related lncRNAs (HRLs) in CM has not been clarified.

Methods: We obtained hypoxia related genes from MSigDB database and subsequently identified HRLs by applying TCGA database. LASSO-univariate and multivariate Cox analysis were used to comprehensively analyze the survival characteristics and HRLs expressions, and a novel HRLs-related prognostic risk model was subsequently established for comprehensive analysis.

Results: The established risk model could evaluate the clinical outcome of CM accurately. The ability of the model-related risk score was also validated as an independent prognostic indicator of CM. Immune infiltration, TMB analysis, drug sensitivity analysis and immunotherapy evaluation were conducted to comprehensively assess the possible causes of the difference in prognosis. The reliability of bioinformatics results was partially verified by RT-qPCR.

Conclusion: We established a new HRLs related risk model and discussed the potential role of hypoxia in the development of CM, which provided a novel basis for CM risk stratification.

INTRODUCTION

Cutaneous melanoma (CM) originates from melanocytes in the skin and is the dominant type of melanoma [1]. Due to its high aggressiveness and significant resistance to chemotherapy drugs, CM accounts for 80% of skin cancer deaths [2]. Although immune checkpoint inhibitors have made great progress in the treatment of melanoma [3], the continued increase in CM incidence and mortality drives us to further explore the mechanisms of melanoma development and potential treatments [4].

Hypoxia is one common feature in many solid tumor types, including CM. Compared with cells in a

physiological state, hypoxic cancer cells increased glycolysis and reduced oxidative phosphorylation [5]. A pooled dataset of melanoma patients found that the presence of hypoxia within the tumor mass was positively associated with poor outcomes in these patients [5]. Hypoxia affects CM development through multiple mechanisms. As one main regulator of hypoxia response, hypoxia-inducible factor (HIF) consists of two subunits, HIF- α and HIF- β , which are able to bind to hypoxia response elements in DNA sequences [6]. A variety of modifications can regulate the adaptation to anoxic environment by controlling the stability and transcriptional activity of HIF-1 α [7]. Through the activation of PI3K, MAPK, NF- κ B and other signaling

pathways that promote tumor development, HIF-1 α responds to growth factor and cytokine stimulation and promotes the survival of cancer cells in hypoxic environments [8]. In addition, when cells trigger HIF-1-dependent pathways under hypoxia conditions, neovascularization occurs [8]. The alteration of HIF-1 α expression level in anoxic microenvironment decreased the expression of melanocyte marker and increased its invasiveness in melanoma cells [9].

In addition to HIF-1 α , some evidence suggests other possible mechanisms by which hypoxia affects CM development. Hypoxic-induced cancer stem cell-like cells (CSCs) can recruit endothelial progenitor cells to construct pathological vasculature [10]. Metabolic reprogramming induced by low oxygen levels also influenced CM development and was associated with prognosis [11, 12]. In addition, hypoxia induces mutations in the gene encoding p53 through the AKT signaling pathway and is associated with poorer prognosis in melanoma patients [13]. Exposure to hypoxia and high glucose concentrations in mouse CM models showed upregulated expression of galectin-3 and prevented tumor cell apoptosis [14]. Elevated levels of Bcl-2 interacting protein 3 (BNIP3) were detected in hypoxic melanoma cells, which was associated with reduced anti-PD-1 therapeutic response due to induced autophagy [15].

Although above evidences suggest a carcinogenesis role of hypoxia in CM. However, oxidative phosphorylation can be enhanced in some types of CM [16]. At the same time, several drugs that inhibit oxidative phosphorylation may be used to target specific subtypes of melanoma [17]. The presence of higher mitochondrial activity in metastatic cancer than in primary cancer also suggests a potential role for oxidative phosphorylation in tumor metastasis [18, 19]. Therefore, it is still necessary to further probe into the significance of hypoxia in the development of CM.

Hypoxia is a prominent feature of the tumor micro-environment (TME) and is also considered to be an important factor in immune escape [20]. The effects of hypoxia on TME include: impaired T cell infiltration, induced immunosuppression and immune tolerance, induced resistance to cell-mediated cytotoxicity and induced lymphocyte killing activity [21, 22]. Hypoxia has received increasing attention by modulating the role of TME in cancer treatment [23]. In melanoma, targeting HIF-1 α has been reported to drive cytotoxic immune effector cells into the tumor and improve combination immunotherapy [20]. In addition, the effect of hypoxia and its metabolites on PD-L1 also suggests its role in CM immunotherapy [24, 25]. Further analysis of hypoxia related TME is of positive significance.

In this study, we subtyped CM patients in the database based on HRLs and subsequently established a corresponding risk model. The effects of the novel risk model on immune infiltration and drug sensitivity were also analyzed to explore the role of hypoxia in the carcinogenesis of CM from a new perspective.

MATERIALS AND METHODS

Collection of CM transcriptome matrices

The gene expression files of CM patient samples were acquired from public database The Cancer Genome Atlas Program (TCGA) under the Perl language environment. Utilizing the Perl script, we extracted the gene expression file of each CM samples and merged into a file. CM clinical information was also extracted from the TCGA database using Perl scripts and subsequently merged into the final file. Considering the lack of information on CM sample's survival, the samples without OS time or less than 0 were deleted. A total of 454 CM samples were screened for subsequent analysis.

Calculation and identification of HRLs

The hypoxia genes were acquired from the MSigDB database (Supplementary Table 1) [26–28]. The coefficient of hypoxia genes and lncRNAs was calculated by using Pearson correlation algorithm. The selection threshold for identifying the HRLs was setting at $|r| > 0.5$, $p < 0.001$.

Prognosis characteristic and consensus clustering subtype exploration

Integrated analysis of survival characteristics and HRLs expression in CM samples, the LASSO-univariate Cox algorithm was conducted to evaluate the prognostic value of HRLs. Moreover, the multivariate Cox analysis of HRLs was used to calculate the CM independent prognostic feature. For CM samples clustering, “ConsensusClusterPlus” script was performed based on the independent prognostic feature according to the optimal classification.

Establishment of HRLs score for CM

Based on the coefficient and expression feature of independent HRLs variables, the HRLs scores were established for CM samples. The optimal survival cutoff helped the CM samples to be classified into the low- and high HRLs score subtypes. To validate the independence of HRLs score for CM prognosis predicting, the training and testing subtypes were divided according to a 7:3 classification threshold by the “caret” package application [29, 30].

Immune microenvironment characteristic estimation

Based on the transcriptome matrices of CM samples, we estimated the immune microenvironment characteristic of CM samples utilizing the ssGSEA algorithm based on “GSVA” script. “ESTIMATE” script was employed to estimate the immune status of CM samples. The KEGG terms were calculated by the “GSVA” algorithm based on the “c2.cp.kegg.v7.2.symbols.gmt” file.

TMB landscape and immunotherapy evaluation

The tumor mutation burden (TMB) files of CM samples were downloaded and extracted from the public TCGA databased using the Perl script. Using the “maftools” script to exhibit the landscape of TMB for CM samples. The IPS file of CM was obtained from The Cancer Immunome Database (TCIA). The Tumor Immune Dysfunction and Exclusion (TIDE) database was used for TIDE score evaluating (<http://tide.dfci.harvard.edu/>).

RT-qPCR analysis

In this study, we employed RT-qPCR to assess the expression levels of the screened prognostic HRLs. RNA

was isolated by TRIZOL (Thermo Fisher Scientific, USA) and Bestar™ qPCR RT Kit (DBI Bioscience, China) was used for cDNA synthesis following the manufacturer’s instructions from HFB4 and A375 cell lines. The relative gene expressions were calculated by the $\Delta\Delta Ct$ method, normalizing to the expression of the reference gene and a control sample (Supplementary Table 2).

Statistical data analysis

All program performance and data analysis were performed in R language environment. For two groups comparison, *T* test and Wilcoxon rank-sum test were used for statistics. One-way ANOVA analysis was applied for statistical analysis among multiple groups. Pearson correlation analysis was used to calculate the correlation between two components and *p* less than 0.05 was regarded as statistically significant.

RESULTS

The HRLs signature construction

The Sankey diagram visualized the relationship between hypoxia related genes and HRLs (Figure 1A). By the

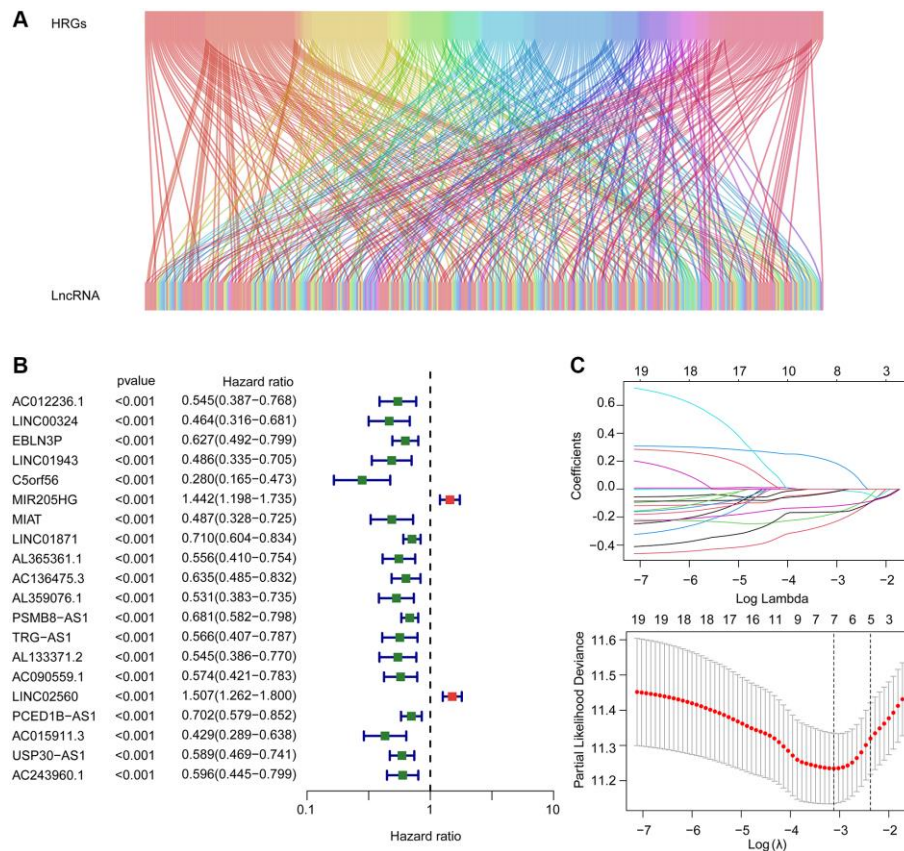


Figure 1. Risk model construction based on the prognostic HRLs in CM. (A) The Sankey diagram shows the detailed connection between HRGs and HRLs. **(B)** Univariate Cox regression analysis of HRLs. **(C)** LASSO regression analysis displays the minimum lambda and optimal coefficients of prognostic HRLs.

least absolute shrinkage and selection operator (LASSO) utilizing, seven prognostic HRLs associated with the overall survival (OS) rate were identified based on the univariate Cox regression (Figure 1B, 1C). The multivariate Cox regression analyses subsequently selected four prognostic HRLs which differentially expressed in tumor and could independently evaluate the prognosis of CM.

Consensus clustering analysis and immune infiltration landscape

The molecular subtypes of CM samples were further explored using 4 prognostic HRLs. An optimal classification of $K = 3$ molecular subtypes was determined for CM patients using consensus clustering. This classification comprised 229, 129, 103 samples in Cluster A, Cluster B and Cluster C respectively, as depicted in the heatmap (Figure 2A). Based on the 4 prognostic HRLs, the result of principal components analysis (PCA) demonstrated a distinct separation of patients into Cluster A, Cluster B and Cluster C (Figure 2B). Kaplan-Meier survival curve analysis showed that CM patients in Cluster B had the highest overall survival (OS), which significantly different from the other two groups of patients. (Figure 2C). Differentially expressed genes (DEGs) between Cluster A and Cluster B were further

enriched in immunodeficiency, antigen processing and presentation, and asthma by KEGG pathway analysis (Figure 2D). DEGs between Cluster B and C were enriched in the receptor signaling pathway, JAK-STAT signaling pathway and toll-like receptor signaling pathway (Figure 2E).

The ESTIMATE assessment algorithm showed patients in Cluster B had the highest ESTIMATE scores, Immune scores, and Stromal scores among the three clusters (Figure 3A–3C). The results of ssGSEA algorithm showed a high level of immune cell enrichment in cluster B patients (Figure 3D). Furthermore, the results of immune function assessment indicated higher immune function scores in Cluster B patients (Figure 3E). IPS results exhibited a best response potential to anti-CTLA-4, anti-PD-1, and the combination of anti-CTLA-4/anti-PD-1 in Cluster B patients, thereby indicating a greater benefit for immunotherapy (Figure 3F–3H). In conclusion, these results provide valuable insights for future individualized precision therapy in CM patients from different subgroups.

HRLs-based risk model development and validation

A risk model was further developed based on 4 prognostic HRLs to assess clinical prognosis. Patients in Cluster C exhibited the worst clinical prognostic

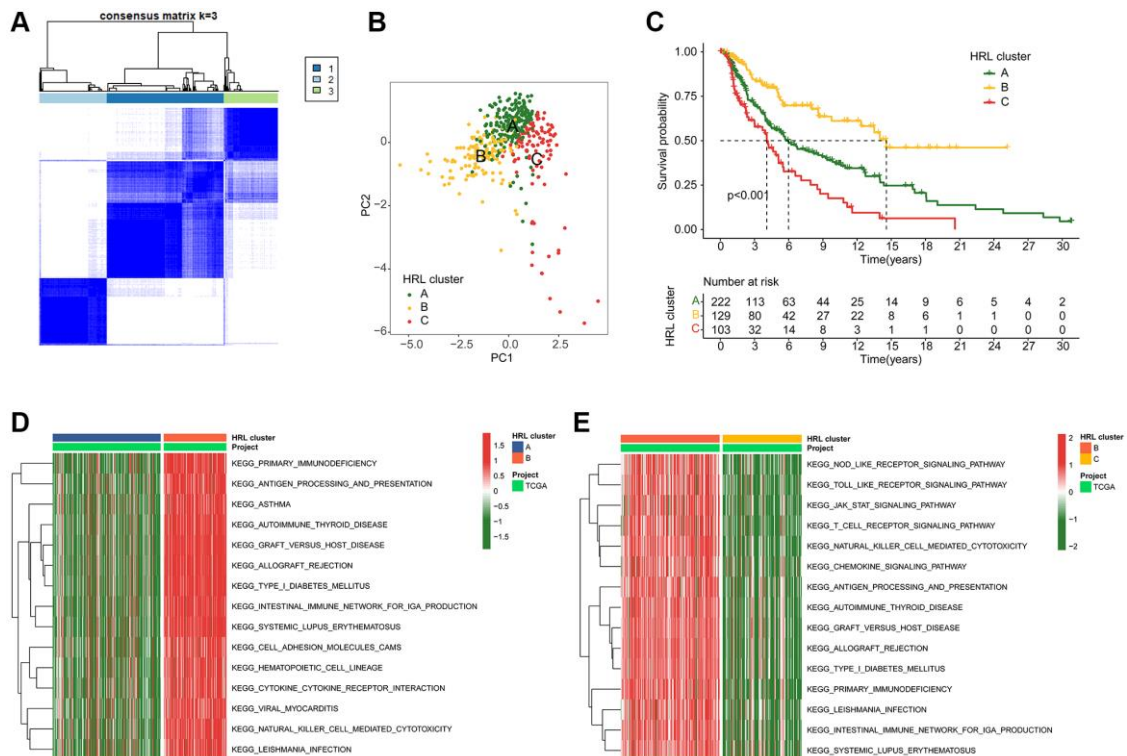


Figure 2. Identification of molecular subtypes for CM. (A) Unsupervised consensus clustering analysis of CM. (B) PCA score plot depicting cluster subgroups. (C) Clinical survival outcomes of CM in the clusters. (D, E) GSVA comparing KEGG signaling pathways among CM subtypes.

outcome, as indicated by the highest risk score among CM cluster subtypes (Figure 4A). The Sankey plot demonstrated the relationship among clusters, risk scores and clinical survival status (Figure 4B). The samples in the established signature were subsequently divided into training cohort ($n = 318$) and test cohort ($n = 136$) using a 7:3 classification ratio. In the entire risk cohort, the CM samples were classified into low- and high-risk groups based on the median risk score. According to the median risk score, CM samples in the entire risk cohort were divided into low-risk and high-risk groups. The results showed that the low-risk score samples had a more optimistic prognosis (Figure 4C). Kaplan-Meier analysis showed that OS rates of with low-risk score CM samples were significantly higher than that with high-risk scores (Figure 4D). Notably, the clinical survival outcomes of CM samples in the

training cohort and test cohort were consistent with those of the entire cohort. CM samples categorized as low-risk had a better OS rate in comparison to the other group (Supplementary Figure 1A, 1B). Furthermore, the time-dependent ROC curves indicated that the area under the curve (AUC) for 1-, 3-, and 5-year survival was 0.726, 0.701, and 0.720 in the training group, and 0.653, 0.595, and 0.691 in the test group, respectively (Supplementary Figure 1C, 1D). In conclusion, these results validated the reliability of established HRLs based risk model in assessing clinical outcomes.

Independent prognostic analysis of HRLs based risk model in CM

The study further explored the independence of the established risk model by combining with the clinical

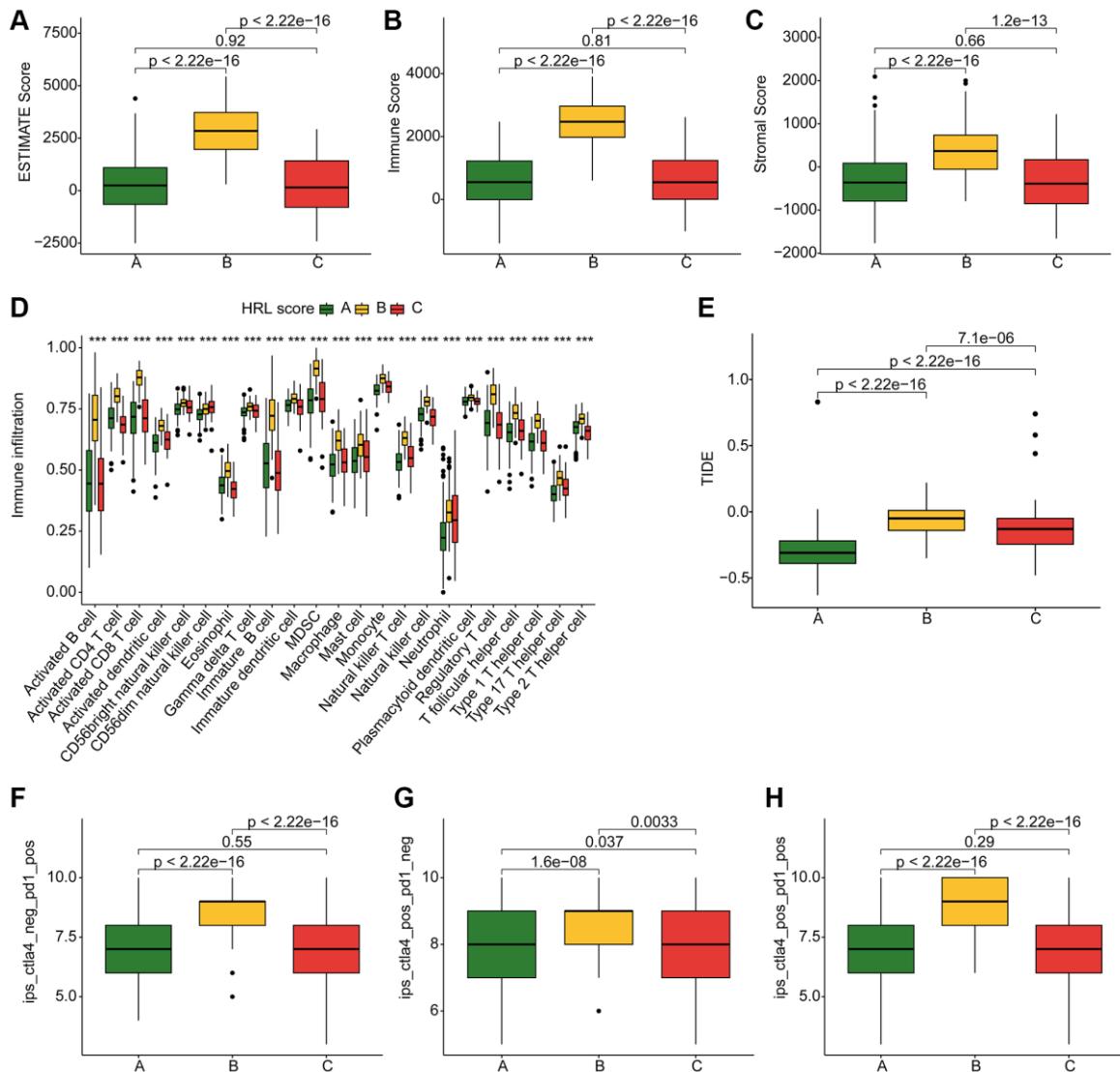


Figure 3. TME landscape and immunotherapy response of CM subtypes. (A–C) ESTIMATE score, Immune score, and Stromal score for Cluster A, B, and C. **(D)** Immune infiltration of 23 types of immune cells in Cluster A, B, and C. **(E)** TIDE score for Cluster A, B, and C. **(F–H)** IPS evaluation demonstrates the response of CM subtypes to PD-1 and CTLA-4.

characteristics. The results indicated a significant difference between fustat, stage (I, II, III, IV) and T stage (T0, T1, T2, T3, T4) (Figure 5A). Univariate Cox analysis in the entire cohort indicated that poor clinical prognosis was associated with the clinical characteristics including age (HR = 1.020 (1.009–1.031), $p < 0.001$), stage (HR = 1.473 (1.217–1.782), $p < 0.001$), T (HR = 1.445 (1.243–1.681), $p < 0.001$), N (HR = 1.443 (1.234–1.688), $p < 0.001$) and HRL score (HR = 1.383 (1.247–1.532), $p < 0.001$) (Figure 5B). The multivariate Cox analysis revealed that age (HR = 1.014 (1.002–1.025), $p = 0.017$), T (HR = 1.367 (1.155–1.619), $p < 0.001$), N (HR = 1.531 (1.199–1.956), $p < 0.001$) and HRL score (HR = 1.247 (1.114–1.396), $p < 0.001$) as CM independent factors (Figure 5B). The results from the training and test

cohorts suggesting that the risk score could be considered as an independent prognostic indicator for CM, which exhibited better predictive value in comparison to other clinical features (Figure 5C, 5D).

The TME landscape and immunotherapy response by risk stratification

The tumor microenvironment (TME) landscape and immunotherapy response analysis by risk stratification were further explored. The ESTIMATE results demonstrated that high-risk score CM patients had lower stromal, immune and overall ESTIMATE scores (Figure 6A–6C). The KEGG pathway analysis indicated that DEGs by risk stratification were enriched in biological processes including cytosolic DNA sensing

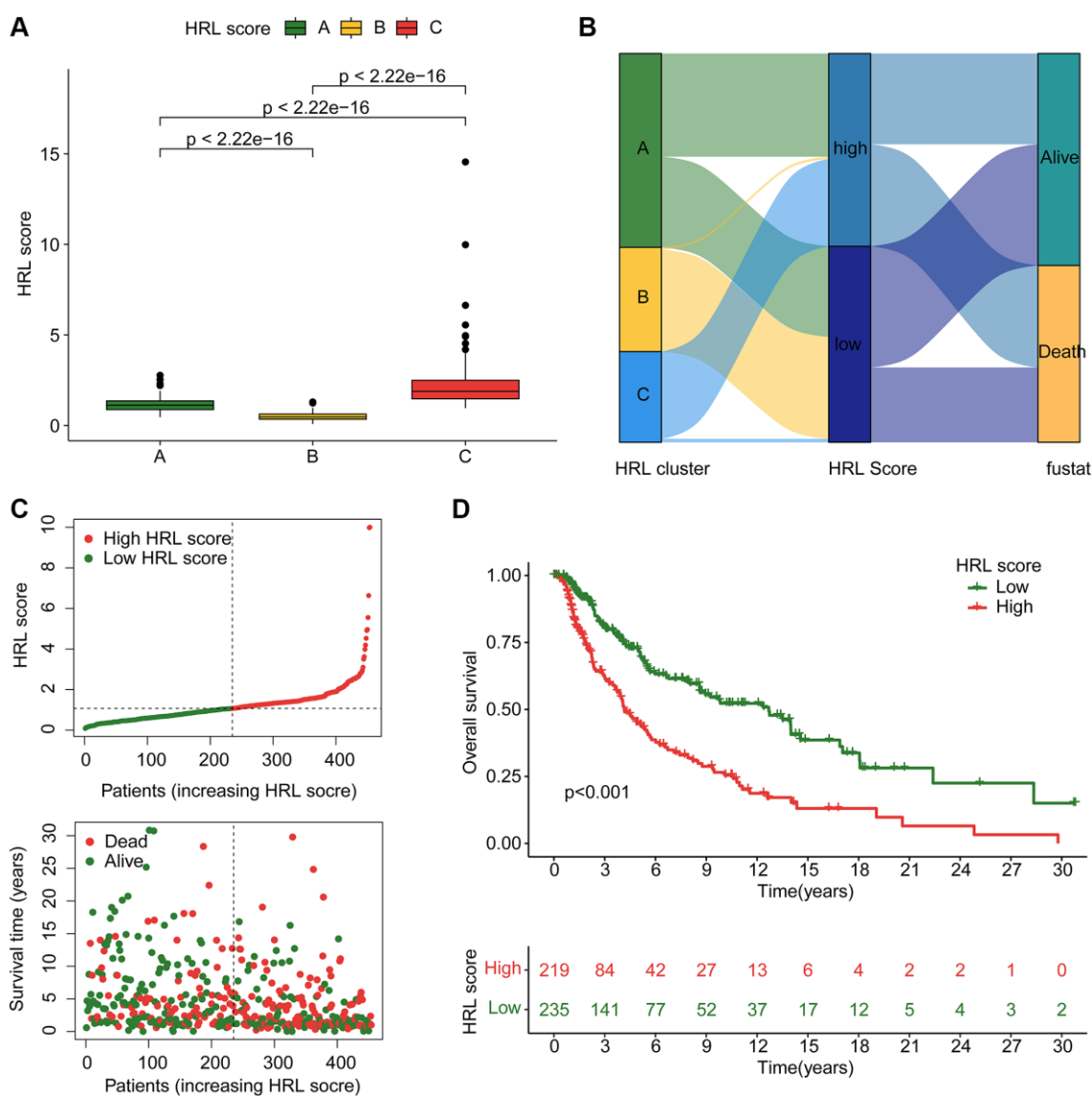


Figure 4. Construction of HRLs risk model in CM. (A) HRL score in CM subtypes. (B) Relationship between HRL score, CM cluster, HRL score, and clinical survival status. (C) Construction of risk model for CM. (D) Clinical prognostic analysis of CM samples in low-risk and high-risk groups.

pathway, the rig-like receptor signaling pathway and toll-like receptor signaling pathway (Figure 6D). The immune infiltration assessment using semi-supervised gene set enrichment analysis (ssGSEA) revealed significant differences in various immune cell populations between the two groups, including activated B cells, CD4⁺ T cells, CD8⁺ T cells, and MDSCs (Figure 6E). The correlation analysis revealed a positive relationship between LINC05260 and EBLN3P expression levels and immune cells, whereas USP30-AS1, LINC00324, and the HRL score

showed a negative association with immune cells (Figure 6F).

Somatic mutation landscape and drug sensitivity analysis

The following results showed a higher tumor mutational burden (TMB) level in low-risk group (Figure 7A). The genetic mutation landscape analysis demonstrated the somatic mutation frequency in both groups. As shown in Figure 7B, 7C, 214 (92.24%) out of 232 low-risk

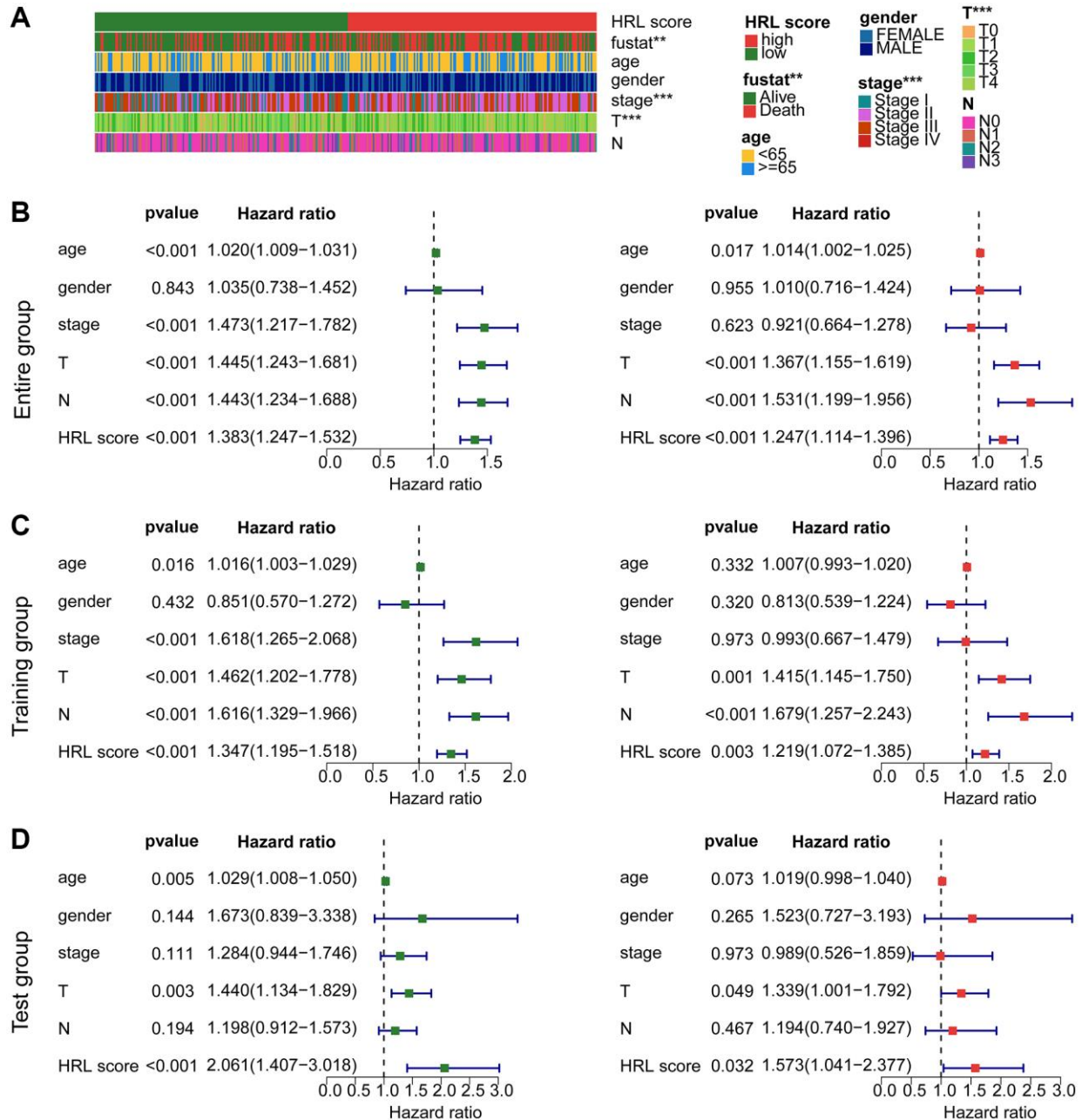


Figure 5. Independent prognosis analysis of risk score and predictive ability evaluation. (A) Clinicopathological characteristics of CM clusters. **(B)** Univariate and multivariate Cox analysis in the entire cohort. **(C)** Independence analysis in the training cohort. **(D)** Independence analysis in the test cohort.

patients and 197 (89.95%) out of 219 high-risk patients exhibited somatic mutations. For the low-risk patients, the mutation frequencies for TTN, MUC16, BRAF, DNAH5, and PCLO were 76%, 72%, 54%, 52%, and 47%, respectively, which were higher than in the other group (Figure 7B, 7C). The TIDE results revealed that low-risk patients had higher TIDE scores (Figure 7D).

Additionally, the IPS results indicated higher sensitivities to PD-1, CTLA-4, or combined treatments for low-risk patients (Figure 7E–7G). Figure 7H–7L displayed the drug sensitivity analysis results, which indicated significantly higher IC50 values of dasatinib, crizotinib, paclitaxel, imatinib, and cyclopamine in the high-risk group. These findings indicated differences in

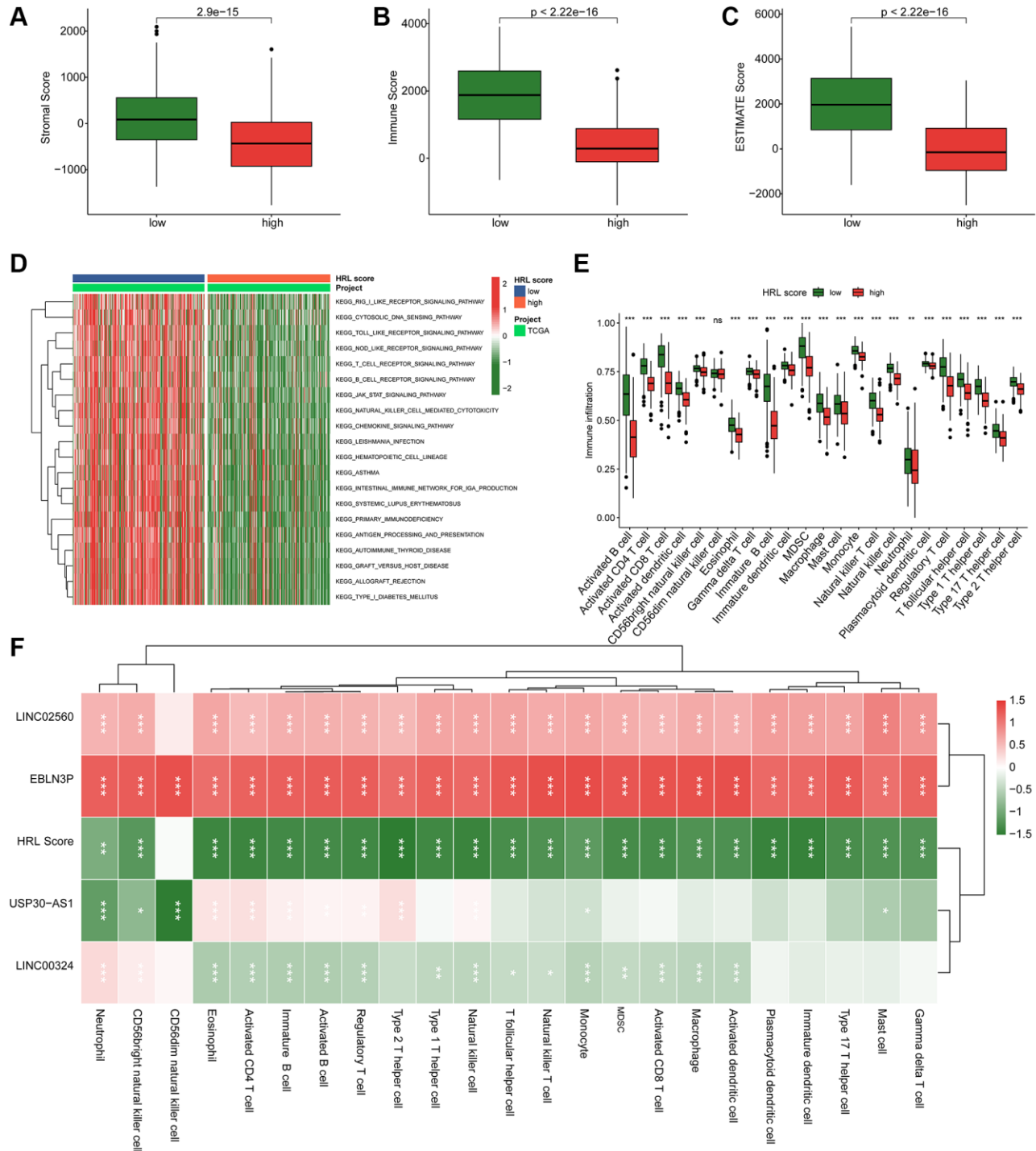


Figure 6. TME landscape and immunotherapy response of CM in the risk subgroups. (A–C) Stromal score, Immune score, and ESTIMATE score. **(D)** GSEA comparing KEGG signaling pathways between low-risk and high-risk groups. **(E)** Estimation of the proportions of 23 immune cells using ssGSEA. **(F)** Correlation analysis of LINC02560, EBLN3P, USP30-AS1, LINC00324 with HRL score and immune cells.

drug sensitivity by risk stratification and provided new insights into precisely targeted therapy for CM patients.

RT-qPCR validation of selected HRLs

We used A375 melanoma cell line for RT-qPCR to verify the bioinformatics screening results in comparison to HFB4 control cell line. As shown Figure 8A–8D, the mRNA expression levels of 4 screened HRLs according to public database showed significant differences with same tendency, which partially verified the reliability of bioinformatics results.

DISCUSSION

In this study, we established a new HRLs-related risk model in CM and comprehensively assessed the possible causes of the difference in prognosis by risk stratification.

Although there is no direct evidence for the function of EBLN3P in CM carcinogenesis, the regulatory effect of EBLN3P on downstream targets may influence the

prognosis of CM. EBLN3P has been reported to regulate the expression of U2AF homology motif kinase 1 (UHMK1) targeting miR-323a-3p [31]. As an RNA processing kinase, UHMK1 controls protein synthesis by regulating the expression and phosphorylation levels of key genes in biological processes [32]. It has been reported in melanoma patients that UHMK1 regulates metabolic reprogramming during targeted therapy through selective mRNA processing and translation, resulting in resistance to targeted therapy [33]. This may be one of the reasons for the prognostic difference by risk stratification.

Despite the lack of in-depth reports on mechanisms, USP30-AS1 has been reported to be associated with melanoma prognosis [34]. One of the main roles of USP30-AS1 is to regulate the expression level of ubiquitin-specific protease 30 (USP30) [35, 36]. USP30 is regulated by post-translational modifications and takes an active part in many cellular events such as infection, autophagy, BAX/ bak-dependent apoptosis, and tumorigenesis [37, 38]. USP30 defects lead to

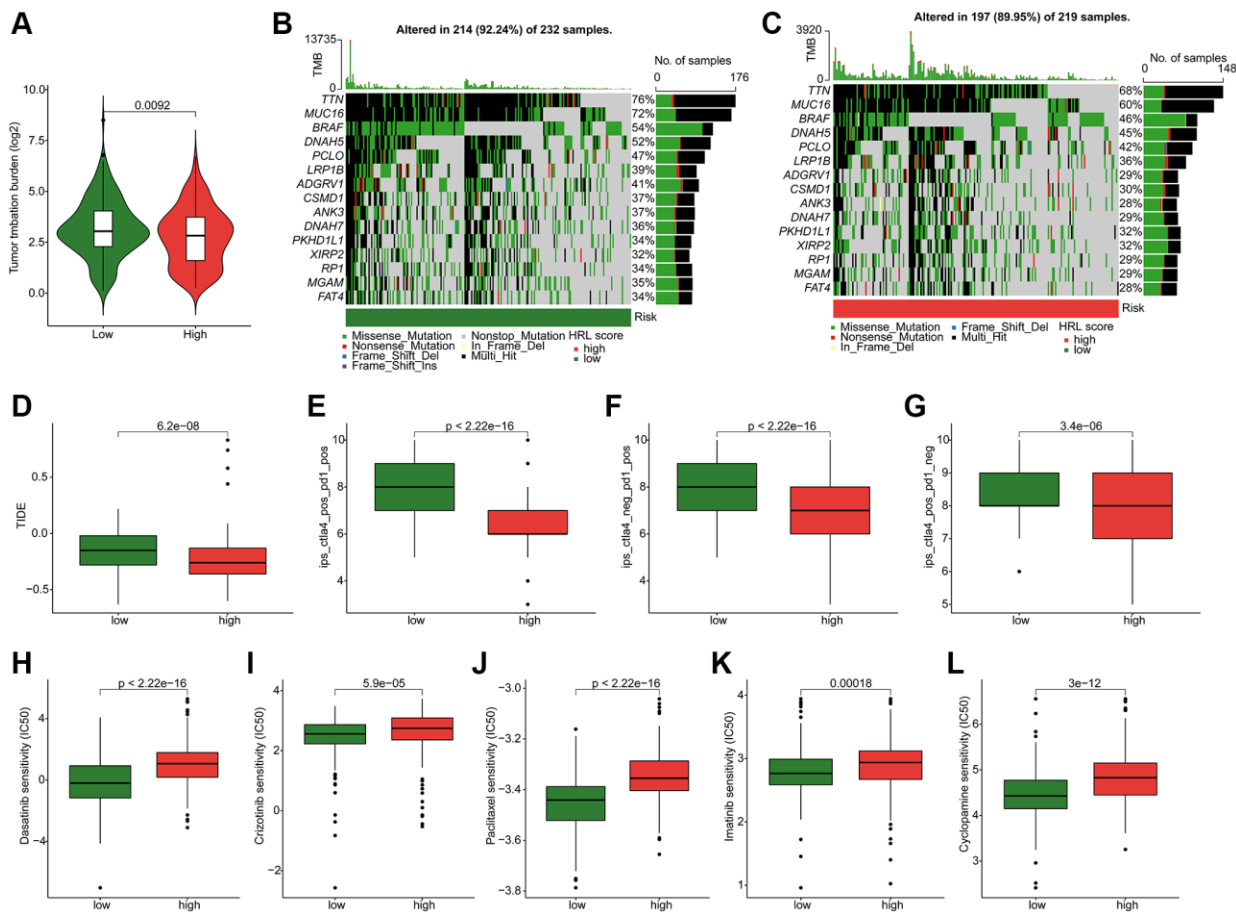


Figure 7. Somatic mutation landscape and drug sensitivity in CM. (A) TMB analysis. (B, C) Genetic mutation frequency in the low-risk and high-risk groups. (D) TIDE scores of CM patients in the low-risk and high-risk groups. (E–G) IPS results in the low-risk and high-risk groups. Distribution of IC50 values in the low-risk and high-risk groups for (H) dasatinib, (I) crizotinib, (J) paclitaxel, (K) imatinib, and (L) cyclopamine.

mitochondrial depletion, which significantly reduces the killing capacity of effector cytotoxic T lymphocytes (CTLs) [39]. Given the significance of CTLs in the development of melanoma [40], mitochondrial dysfunction caused by the USP30-AS1/USP30 axis may be an important cause.

In addition to its classic function of complex ceRNA network forming, LINC00324 can also bind RNA-binding proteins and recruit transcription factors in order to regulate multiple downstream gene expressions [41]. Although no relevant studies have been conducted in CM, LINC00324 has been shown to be overexpressed in a variety of cancer types and to be associated with pathologic features and

risk stratification [42]. Unlike most tumor types, we observed a significant reduction in LINC00324 mRNA level in the A375 melanoma cell line compared to the HFB4 control cell line, which is in line with the observation in breast cancer [43]. LINC00324 affects multiple miRNA/mRNA axes and is involved in the regulation of various signaling pathways, such as miR-139-5p/IGF1R, miR-615-5p/AKT1, Mir-799-5p/STAT3, and miR-10b-5p/E-cadherin [44]. Among them, miR-10b-5p was involved in the inhibition of E-cadherin during EMT [45, 46]. By regulating miR-10b-5p, LINC00324 can promote the expression level of E-cadherin, thereby inhibiting tumor progression [46]. This may partially explain the correlation between LINC00324 and prognosis in CM.

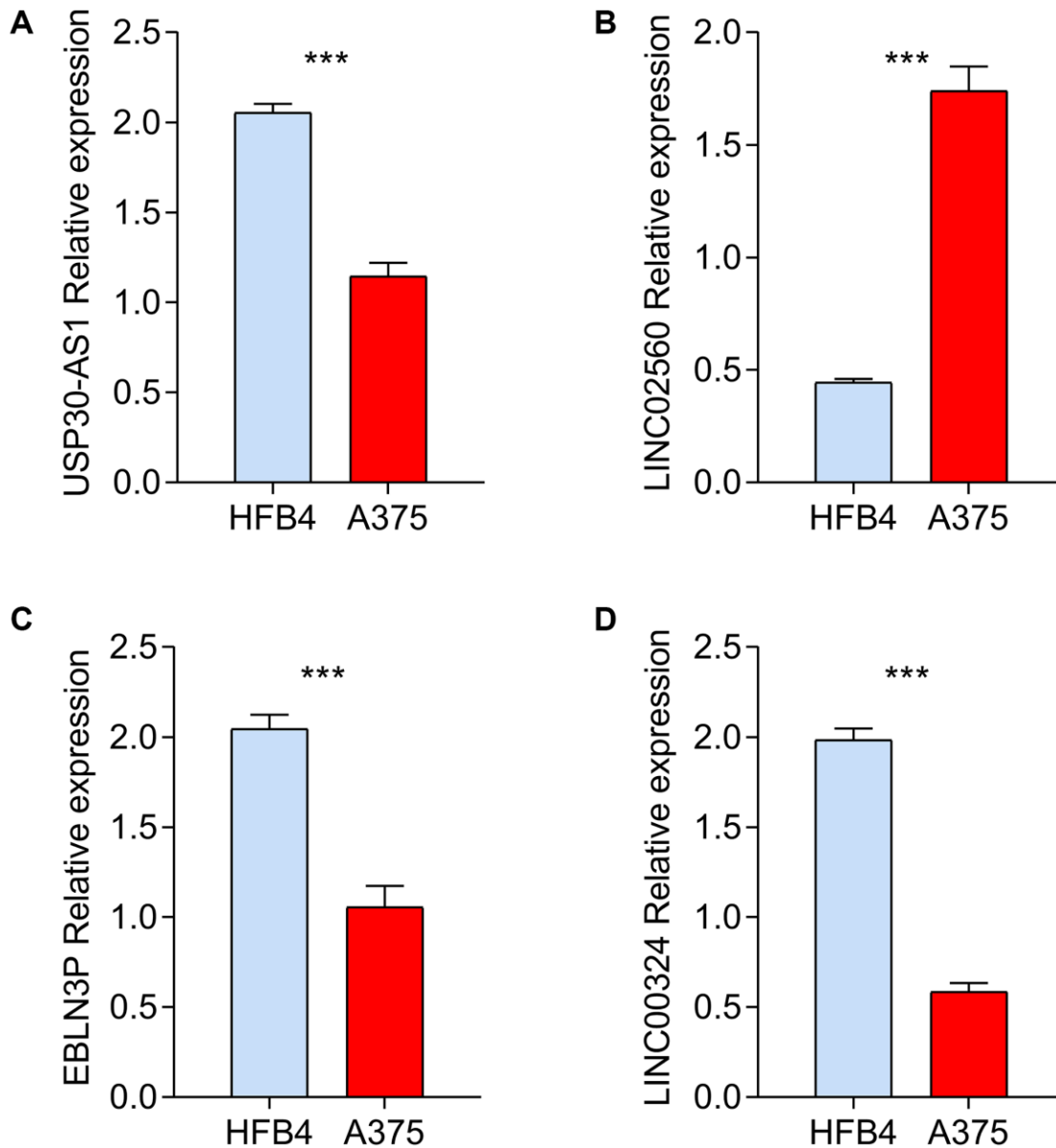


Figure 8. *In vitro* validation of prognostic HRLs in HFB4 and A375 cell lines. RT-qPCR was used to test the mRNA levels of USP30-AS1 (A), LINC02560 (B), EBLN3P (C) and LINC00324 (D) in HFB4 and A375 cell lines.

The adaptive mechanisms by which cancer cells survive prolonged oxygen deprivation often led to the emergence of drug resistance. Its mechanisms include HIF-1 α induced tight packing of genetic material, decreased mitochondrial DNA damage levels of organelles, decreased reactive oxygen species levels, and activation of pro-survival pathways [12, 47, 48]. Our results again suggest the guiding value of hypoxia related prognostic models for immune response and sensitivity to specific chemotherapy drugs. Therefore, new therapeutic strategies targeting hypoxic tumor microenvironments, including HIF-1 α inhibitors, hypoxia relief, oxygen sensitive therapy, etc., have clinical application potential of CM [49]. In addition, hypoxia can inhibit CTL cytotoxic activity, thus affecting immune response [50]. Our IPS results suggest poor response to immunotherapy in the high-risk group. This was consistent with the trend of reduced levels of immune components in high-risk patients.

In summary, we establish a novel risk model related to HRLs and provide a new basis for CM risk stratification and target screening. Limited by the conditions, most of the conclusions in this paper are correlation studies rather than causation studies. Further *in vitro* and *in vivo* experiments can better reveal the effect of selected HRLs on the pathogenesis of CM in the future. Additionally, the sources of data in the database also lack of ethnic diversity and sample size. Further multi-center studies worldwide investigation will help us to know better about the role of HRLs in tumorigenesis.

AUTHOR CONTRIBUTIONS

Z.Y. conceived and designed the study. C.L. and J.Y. contributed to the data analysis and composed this manuscript. L.C. completed the experiment. C.L. and J.Y. contributed tables and diagrams to this manuscript. All authors contributed to the article and approved the submitted version.

CONFLICTS OF INTEREST

The authors declare no conflicts of interest related to this study.

FUNDING

This study was supported by Shenzhen Longgang District Science and Technology Development Special Funds (LGKCYLWS2018000172).

REFERENCES

1. Schadendorf D, Fisher DE, Garbe C, Gershenwald JE, Grob JJ, Halpern A, Herlyn M, Marchetti MA,

- McArthur G, Ribas A, Roesch A, Hauschild A. Melanoma. *Nat Rev Dis Primers*. 2015; 1:15003. <https://doi.org/10.1038/nrdp.2015.3> PMID:27188223
2. Vedung S, af Ekenstam F. Osteocutaneous grafting from the forearm to the foot. Case report. *Scand J Plast Reconstr Surg Hand Surg*. 1991; 25:177–9. <https://doi.org/10.3109/02844319109111280> PMID:1682996
3. Furue M, Ito T, Wada N, Wada M, Kadono T, Uchi H. Melanoma and Immune Checkpoint Inhibitors. *Curr Oncol Rep*. 2018; 20:29. <https://doi.org/10.1007/s11912-018-0676-z> PMID:29569208
4. Siegel RL, Miller KD, Jemal A. Cancer statistics, 2019. *CA Cancer J Clin*. 2019; 69:7–34. <https://doi.org/10.3322/caac.21551> PMID:30620402
5. Lartigau E, Randrianarivelo H, Avril MF, Margulis A, Spatz A, Eschwège F, Guichard M. Intratumoral oxygen tension in metastatic melanoma. *Melanoma Res*. 1997; 7:400–6. <https://doi.org/10.1097/00008390-199710000-00006> PMID:9429223
6. Huang Y, Lin D, Taniguchi CM. Hypoxia inducible factor (HIF) in the tumor microenvironment: friend or foe? *Sci China Life Sci*. 2017; 60:1114–24. <https://doi.org/10.1007/s11427-017-9178-y> PMID:29039125
7. Masoud GN, Li W. HIF-1 α pathway: role, regulation and intervention for cancer therapy. *Acta Pharm Sin B*. 2015; 5:378–89. <https://doi.org/10.1016/j.apsb.2015.05.007> PMID:26579469
8. Schito L. Hypoxia-Dependent Angiogenesis and Lymphangiogenesis in Cancer. *Adv Exp Med Biol*. 2019; 1136:71–85. https://doi.org/10.1007/978-3-030-12734-3_5 PMID:31201717
9. Widmer DS, Hoek KS, Cheng PF, Eichhoff OM, Biedermann T, Raaijmakers MIG, Hemmi S, Dummer R, Levesque MP. Hypoxia contributes to melanoma heterogeneity by triggering HIF1 α -dependent phenotype switching. *J Invest Dermatol*. 2013; 133:2436–43. <https://doi.org/10.1038/jid.2013.115> PMID:23474946
10. Klimkiewicz K, Weglarczyk K, Collet G, Paprocka M, Guichard A, Sarna M, Jozkowicz A, Dulak J, Sarna T, Grillon C, Kieda C. A 3D model of tumour angiogenic microenvironment to monitor hypoxia effects on cell interactions and cancer stem cell selection. *Cancer Lett*. 2017; 396:10–20.

<https://doi.org/10.1016/j.canlet.2017.03.006>
PMID:[28288873](https://pubmed.ncbi.nlm.nih.gov/28288873/)

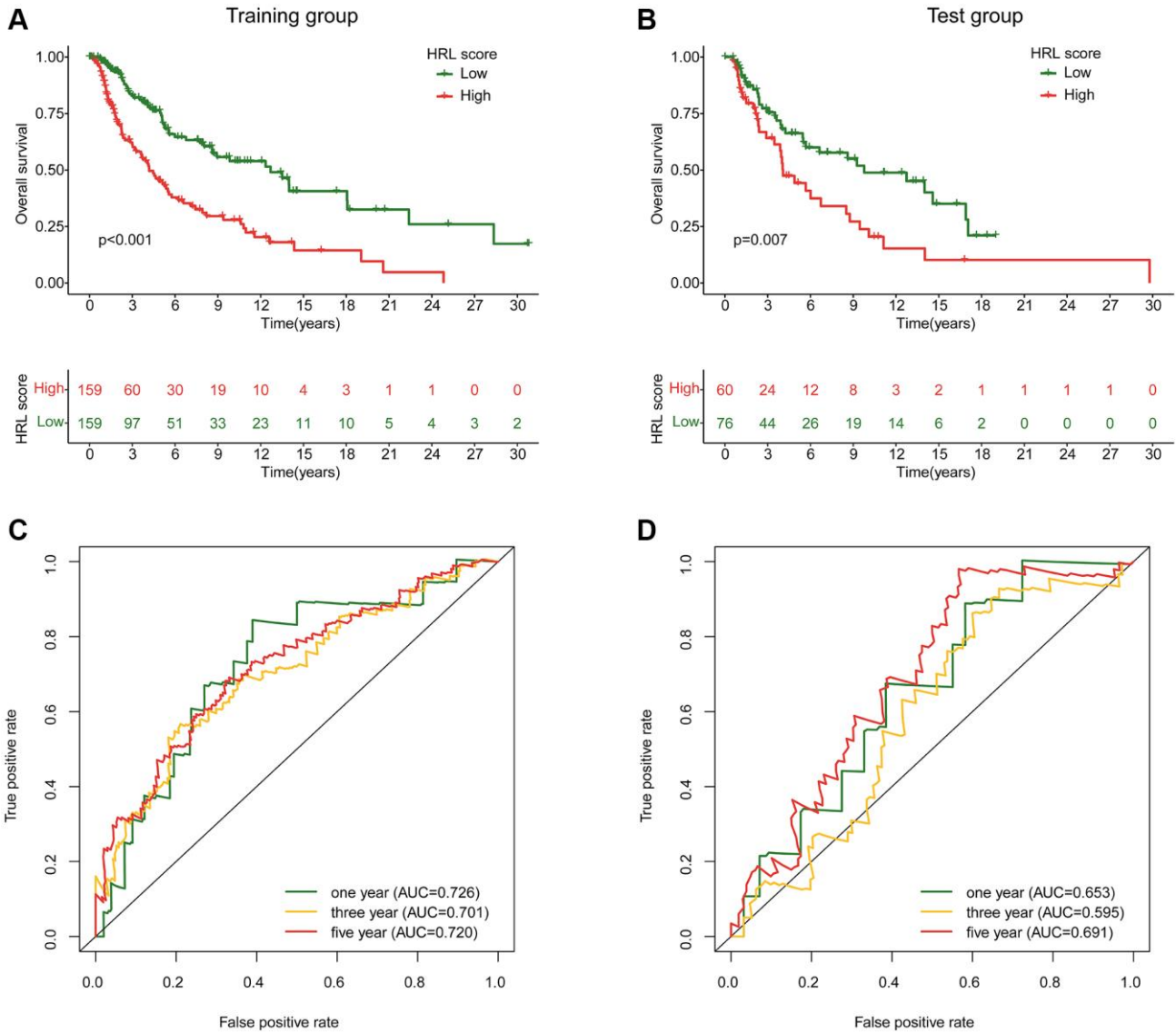
11. Trojan SE, Piwowar M, Ostrowska B, Laidler P, Kocemba-Pilarczyk KA. Analysis of Malignant Melanoma Cell Lines Exposed to Hypoxia Reveals the Importance of PFKFB4 Overexpression for Disease Progression. *Anticancer Res.* 2018; 38:6745–52.
<https://doi.org/10.21873/anticancerres.13044>
PMID:[30504385](https://pubmed.ncbi.nlm.nih.gov/30504385/)
12. Zhuo M, Gorgun FM, Tyler DS, Englander EW. Hypoxia potentiates the capacity of melanoma cells to evade cisplatin and doxorubicin cytotoxicity via glycolytic shift. *FEBS Open Bio.* 2020; 10:789–801.
<https://doi.org/10.1002/2211-5463.12830>
PMID:[32134564](https://pubmed.ncbi.nlm.nih.gov/32134564/)
13. Leszczynska KB, Foskolou IP, Abraham AG, Anbalagan S, Tellier C, Haider S, Span PN, O'Neill EE, Buffa FM, Hammond EM. Hypoxia-induced p53 modulates both apoptosis and radiosensitivity via AKT. *J Clin Invest.* 2015; 125:2385–98.
<https://doi.org/10.1172/JCI80402>
PMID:[25961455](https://pubmed.ncbi.nlm.nih.gov/25961455/)
14. Bacchi PS, Bloise AC, Bustos SO, Zimmermann L, Chammas R, Rabbani SR. Metabolism under hypoxia in Tm1 murine melanoma cells is affected by the presence of galectin-3, a metabolomics approach. *Springerplus.* 2014; 3:470.
<https://doi.org/10.1186/2193-1801-3-470>
PMID:[25221735](https://pubmed.ncbi.nlm.nih.gov/25221735/)
15. Buart S, Terry S, Noman MZ, Lanoy E, Boutros C, Fogel P, Dessen P, Meurice G, Gaston-Mathé Y, Vielh P, Roy S, Routier E, Marty V, et al. Transcriptional response to hypoxic stress in melanoma and prognostic potential of GBE1 and BNIP3. *Oncotarget.* 2017; 8:108786–801.
<https://doi.org/10.18632/oncotarget.22150>
PMID:[29312568](https://pubmed.ncbi.nlm.nih.gov/29312568/)
16. Haq R, Shoag J, Andreu-Perez P, Yokoyama S, Edelman H, Rowe GC, Frederick DT, Hurley AD, Nellore A, Kung AL, Wargo JA, Song JS, Fisher DE, et al. Oncogenic BRAF regulates oxidative metabolism via PGC1 α and MITF. *Cancer Cell.* 2013; 23:302–15.
<https://doi.org/10.1016/j.ccr.2013.02.003>
PMID:[23477830](https://pubmed.ncbi.nlm.nih.gov/23477830/)
17. Ashton TM, McKenna WG, Kunz-Schughart LA, Higgins GS. Oxidative Phosphorylation as an Emerging Target in Cancer Therapy. *Clin Cancer Res.* 2018; 24:2482–90.
<https://doi.org/10.1158/1078-0432.CCR-17-3070>
PMID:[29420223](https://pubmed.ncbi.nlm.nih.gov/29420223/)
18. Porporato PE, Payen VL, Pérez-Escuredo J, De Saedeleer CJ, Danhier P, Copetti T, Dhup S, Tardy M, Vazeille T, Bouzin C, Feron O, Michiels C, Gallez B, Sonveaux P. A mitochondrial switch promotes tumor metastasis. *Cell Rep.* 2014; 8:754–66.
<https://doi.org/10.1016/j.celrep.2014.06.043>
PMID:[25066121](https://pubmed.ncbi.nlm.nih.gov/25066121/)
19. LeBleu VS, O'Connell JT, Gonzalez Herrera KN, Wikman H, Pantel K, Haigis MC, de Carvalho FM, Damascena A, Domingos Chinen LT, Rocha RM, Asara JM, Kalluri R. PGC-1 α mediates mitochondrial biogenesis and oxidative phosphorylation in cancer cells to promote metastasis. *Nat Cell Biol.* 2014; 16:992–1003.
<https://doi.org/10.1038/ncb3039>
PMID:[25241037](https://pubmed.ncbi.nlm.nih.gov/25241037/)
20. Lequeux A, Noman MZ, Xiao M, Van Moer K, Hasmim M, Benoit A, Bosseler M, Viry E, Arakelian T, Berchem G, Chouaib S, Janji B. Targeting HIF-1 alpha transcriptional activity drives cytotoxic immune effector cells into melanoma and improves combination immunotherapy. *Oncogene.* 2021; 40:4725–35.
<https://doi.org/10.1038/s41388-021-01846-x>
PMID:[34155342](https://pubmed.ncbi.nlm.nih.gov/34155342/)
21. Vignali PDA, DePeaux K, Watson MJ, Ye C, Ford BR, Lontos K, McGaa NK, Scharping NE, Menk AV, Robson SC, Poholek AC, Rivadeneira DB, Delgoffe GM. Hypoxia drives CD39-dependent suppressor function in exhausted T cells to limit antitumor immunity. *Nat Immunol.* 2023; 24:267–79.
<https://doi.org/10.1038/s41590-022-01379-9>
PMID:[36543958](https://pubmed.ncbi.nlm.nih.gov/36543958/)
22. Chouaib S, Noman MZ, Kosmatopoulos K, Curran MA. Hypoxic stress: obstacles and opportunities for innovative immunotherapy of cancer. *Oncogene.* 2017; 36:439–45.
<https://doi.org/10.1038/ncr.2016.225>
PMID:[27345407](https://pubmed.ncbi.nlm.nih.gov/27345407/)
23. Jing X, Yang F, Shao C, Wei K, Xie M, Shen H, Shu Y. Role of hypoxia in cancer therapy by regulating the tumor microenvironment. *Mol Cancer.* 2019; 18:157.
<https://doi.org/10.1186/s12943-019-1089-9>
PMID:[31711497](https://pubmed.ncbi.nlm.nih.gov/31711497/)
24. Lv H, Lv G, Chen C, Zong Q, Jiang G, Ye D, Cui X, He Y, Xiang W, Han Q, Tang L, Yang W, Wang H. NAD⁺ Metabolism Maintains Inducible PD-L1 Expression to Drive Tumor Immune Evasion. *Cell Metab.* 2021; 33:110–27.e5.
<https://doi.org/10.1016/j.cmet.2020.10.021>
PMID:[33171124](https://pubmed.ncbi.nlm.nih.gov/33171124/)
25. Noman MZ, Desantis G, Janji B, Hasmim M, Karray S, Dessen P, Bronte V, Chouaib S. PD-L1 is a novel direct target of HIF-1 α , and its blockade under hypoxia enhanced MDSC-mediated T cell activation. *J Exp Med.* 2014; 211:781–90.

- <https://doi.org/10.1084/jem.20131916>
PMID:[24778419](https://pubmed.ncbi.nlm.nih.gov/24778419/)
26. Wang G, Sun Y, Xu Q. The development and experimental validation of hypoxia-related long noncoding RNAs prognostic signature in predicting prognosis and immunotherapy of cutaneous melanoma. *Aging (Albany NY)*. 2023; 15:11918–39.
<https://doi.org/10.18632/aging.205157>
PMID:[37921852](https://pubmed.ncbi.nlm.nih.gov/37921852/)
27. Subramanian A, Tamayo P, Mootha VK, Mukherjee S, Ebert BL, Gillette MA, Paulovich A, Pomeroy SL, Golub TR, Lander ES, Mesirov JP. Gene set enrichment analysis: a knowledge-based approach for interpreting genome-wide expression profiles. *Proc Natl Acad Sci U S A*. 2005; 102:15545–50.
<https://doi.org/10.1073/pnas.0506580102>
PMID:[16199517](https://pubmed.ncbi.nlm.nih.gov/16199517/)
28. Mootha VK, Lindgren CM, Eriksson KF, Subramanian A, Sihag S, Lehar J, Puigserver P, Carlsson E, Ridderstråle M, Laurila E, Houstis N, Daly MJ, Patterson N, et al. PGC-1alpha-responsive genes involved in oxidative phosphorylation are coordinately downregulated in human diabetes. *Nat Genet*. 2003; 34:267–73.
<https://doi.org/10.1038/ng1180>
PMID:[12808457](https://pubmed.ncbi.nlm.nih.gov/12808457/)
29. Hu M, Chong R, Liu W, Liu S, Liu X. Characteristic of molecular subtype based on lysosome-associated genes reveals clinical prognosis and immune infiltration of gastric cancer. *Front Oncol*. 2023; 13:1155418.
<https://doi.org/10.3389/fonc.2023.1155418>
PMID:[37197421](https://pubmed.ncbi.nlm.nih.gov/37197421/)
30. Qi C, Ma J, Sun J, Wu X, Ding J. The role of molecular subtypes and immune infiltration characteristics based on disulfidptosis-associated genes in lung adenocarcinoma. *Aging (Albany NY)*. 2023; 15:5075–95.
<https://doi.org/10.18632/aging.204782>
PMID:[37315289](https://pubmed.ncbi.nlm.nih.gov/37315289/)
31. Xu XH, Song W, Li JH, Huang ZQ, Liu YF, Bao Q, Shen ZW. Long Non-coding RNA EBLN3P Regulates UHMK1 Expression by Sponging miR-323a-3p and Promotes Colorectal Cancer Progression. *Front Med (Lausanne)*. 2021; 8:651600.
<https://doi.org/10.3389/fmed.2021.651600>
PMID:[34109193](https://pubmed.ncbi.nlm.nih.gov/34109193/)
32. Arfelli VC, Chang YC, Bagnoli JW, Kerbs P, Ciamponi FE, Paz LMD, Pankivskiy S, de Matha Salone J, Maucuer A, Massirer KB, Enard W, Kuster B, Greif PA, Archangelo LF. UHMK1 is a novel splicing regulatory kinase. *J Biol Chem*. 2023; 299:103041.
<https://doi.org/10.1016/j.jbc.2023.103041>
PMID:[36803961](https://pubmed.ncbi.nlm.nih.gov/36803961/)
33. Smith LK, Parmenter T, Kleinschmidt M, Kusnadi EP, Kang J, Martin CA, Lau P, Patel R, Lorent J, Papadopoulos D, Trigos A, Ward T, Rao AD, et al. Adaptive translational reprogramming of metabolism limits the response to targeted therapy in BRAF(V600) melanoma. *Nat Commun*. 2022; 13:1100.
<https://doi.org/10.1038/s41467-022-28705-x>
PMID:[35232962](https://pubmed.ncbi.nlm.nih.gov/35232962/)
34. Zhang M, Yang L, Wang Y, Zuo Y, Chen D, Guo X. Comprehensive prediction of immune microenvironment and hot and cold tumor differentiation in cutaneous melanoma based on necroptosis-related lncRNA. *Sci Rep*. 2023; 13:7299.
<https://doi.org/10.1038/s41598-023-34238-0>
PMID:[37147395](https://pubmed.ncbi.nlm.nih.gov/37147395/)
35. Wang N, Li J, Xin Q, Xu N. USP30-AS1 contributes to mitochondrial quality control in glioblastoma cells. *Biochem Biophys Res Commun*. 2021; 581:31–7.
<https://doi.org/10.1016/j.bbrc.2021.10.006>
PMID:[34653676](https://pubmed.ncbi.nlm.nih.gov/34653676/)
36. Zhou W, Xu S, Deng T, Zhou R, Wang C. lncRNA USP30-AS1 promotes the survival of acute myeloid leukemia cells by cis-regulating USP30 and ANKRD13A. *Hum Cell*. 2022; 35:360–78.
<https://doi.org/10.1007/s13577-021-00636-7>
PMID:[34694569](https://pubmed.ncbi.nlm.nih.gov/34694569/)
37. Wang F, Gao Y, Zhou L, Chen J, Xie Z, Ye Z, Wang Y. USP30: Structure, Emerging Physiological Role, and Target Inhibition. *Front Pharmacol*. 2022; 13:851654.
<https://doi.org/10.3389/fphar.2022.851654>
PMID:[35308234](https://pubmed.ncbi.nlm.nih.gov/35308234/)
38. Gu L, Zhu Y, Lin X, Lu B, Zhou X, Zhou F, Zhao Q, Prochownik EV, Li Y. The IKKβ-USP30-ACLY Axis Controls Lipogenesis and Tumorigenesis. *Hepatology*. 2021; 73:160–74.
<https://doi.org/10.1002/hep.31249>
PMID:[32221968](https://pubmed.ncbi.nlm.nih.gov/32221968/)
39. Lisci M, Barton PR, Randzavola LO, Ma CY, Marchingo JM, Cantrell DA, Paupe V, Prudent J, Stinchcombe JC, Griffiths GM. Mitochondrial translation is required for sustained killing by cytotoxic T cells. *Science*. 2021; 374:eabe9977.
<https://doi.org/10.1126/science.abe9977>
PMID:[34648346](https://pubmed.ncbi.nlm.nih.gov/34648346/)
40. Chapuis AG, Lee SM, Thompson JA, Roberts IM, Margolin KA, Bhatia S, Sloan HL, Lai I, Wagener F, Shibuya K, Cao J, Wolchok JD, Greenberg PD, Yee C. Combined IL-21-primed polyclonal CTL plus CTLA4 blockade controls refractory metastatic melanoma in a patient. *J Exp Med*. 2016; 213:1133–9.
<https://doi.org/10.1084/jem.20152021>
PMID:[27242164](https://pubmed.ncbi.nlm.nih.gov/27242164/)

41. Chen H, Wei L, Luo M, Wang X, Zhu C, Huang H, Liu X, Lu H, Zhong Y. LINC00324 suppresses apoptosis and autophagy in nasopharyngeal carcinoma through upregulation of PAD4 and activation of the PI3K/AKT signaling pathway. *Cell Biol Toxicol.* 2022; 38:995–1011.
<https://doi.org/10.1007/s10565-021-09632-x>
PMID:[34322788](https://pubmed.ncbi.nlm.nih.gov/34322788/)
42. Xia Q, Shen J, Wang Q, Ke Y, Yan Q, Li H, Zhang D, Duan S. LINC00324 in cancer: Regulatory and therapeutic implications. *Front Oncol.* 2022; 12:1039366.
<https://doi.org/10.3389/fonc.2022.1039366>
PMID:[36620587](https://pubmed.ncbi.nlm.nih.gov/36620587/)
43. Singh RP, Jeyaraju DV, Voisin V, Hurren R, Xu C, Hawley JR, Barghout SH, Khan DH, Gronda M, Wang X, Jitkova Y, Sharon D, Liyanagae S, et al. Disrupting Mitochondrial Copper Distribution Inhibits Leukemic Stem Cell Self-Renewal. *Cell Stem Cell.* 2020; 26:926–37.e10.
<https://doi.org/10.1016/j.stem.2020.04.010>
PMID:[32416059](https://pubmed.ncbi.nlm.nih.gov/32416059/)
44. Ghafouri-Fard S, Safarzadeh A, Hussien BM, Taheri M, Rashnoo F. A concise review on the role of LINC00324 in different cancers. *Pathol Res Pract.* 2022; 240:154192.
<https://doi.org/10.1016/j.prp.2022.154192>
PMID:[36399929](https://pubmed.ncbi.nlm.nih.gov/36399929/)
45. Stuelten CH, Parent CA, Montell DJ. Cell motility in cancer invasion and metastasis: insights from simple model organisms. *Nat Rev Cancer.* 2018; 18:296–312.
<https://doi.org/10.1038/nrc.2018.15>
PMID:[29546880](https://pubmed.ncbi.nlm.nih.gov/29546880/)
46. Wang B, Zhang Y, Zhang H, Lin F, Tan Q, Qin Q, Bao W, Liu Y, Xie J, Zeng Q. Long intergenic non-protein coding RNA 324 prevents breast cancer progression by modulating miR-10b-5p. *Aging (Albany NY).* 2020; 12:6680–99.
<https://doi.org/10.18632/aging.103021>
PMID:[32305959](https://pubmed.ncbi.nlm.nih.gov/32305959/)
47. Wittgen HG, van Kempen LC. Reactive oxygen species in melanoma and its therapeutic implications. *Melanoma Res.* 2007; 17:400–9.
<https://doi.org/10.1097/CMR.0b013e3282f1d312>
PMID:[17992124](https://pubmed.ncbi.nlm.nih.gov/17992124/)
48. Brown JM, Wilson WR. Exploiting tumour hypoxia in cancer treatment. *Nat Rev Cancer.* 2004; 4:437–47.
<https://doi.org/10.1038/nrc1367>
PMID:[15170446](https://pubmed.ncbi.nlm.nih.gov/15170446/)
49. Dratkiewicz E, Simiczyjew A, Mazurkiewicz J, Ziętek M, Matkowski R, Nowak D. Hypoxia and Extracellular Acidification as Drivers of Melanoma Progression and Drug Resistance. *Cells.* 2021; 10:862.
<https://doi.org/10.3390/cells10040862>
PMID:[33918883](https://pubmed.ncbi.nlm.nih.gov/33918883/)
50. Tittarelli A, Janji B, Van Moer K, Noman MZ, Chouaib S. The Selective Degradation of Synaptic Connexin 43 Protein by Hypoxia-induced Autophagy Impairs Natural Killer Cell-mediated Tumor Cell Killing. *J Biol Chem.* 2015; 290:23670–9.
<https://doi.org/10.1074/jbc.M115.651547>
PMID:[26221040](https://pubmed.ncbi.nlm.nih.gov/26221040/)

SUPPLEMENTARY MATERIALS

Supplementary Figure



Supplementary Figure 1. Clinical prognostic analysis of CM samples in the low-risk and high-risk groups in the (A) Training cohort and (B) Test cohort. (C) ROC curve in the training cohort and (D) Test cohort.

Supplementary Tables

Please browse Full Text version to see the data of Supplementary Table 1.

Supplementary Table 1. The gene list of hypoxia related genes signature.

Supplementary Table 2. The primer sequences of hypoxia-related lncRNAs.

LINC00324	Forward primer	TGTGGATGACAGTGTTCTGGG
	Reverse primer	ACGCTGACCAGAAACCGTAG
USP30-AS1	Forward primer	GAACGTAGACCGCAGGACAG
	Reverse primer	GACGTGGTCCGTCAGCTATT
EBLN3P	Forward primer	TGAGGACCGAGTAGTCCTGG
	Reverse primer	TCCTATGCCCAGATCGTCCA
LINC02560	Forward primer	CACTCTACCAGCTTGGAGCC
	Reverse primer	AATCAGCAGACCAGATGCCC